XVIII International Conference on Water Resources
CMWR 2010
J. Carrera (Ed)

FLUID-FLUID INTERFACIAL AREA UNDER NON-EQUILIBRIUM CONDITIONS

Vahid Joekar-Niasar*, S. Majid Hassanizadeh †

*Department of Earth Sciences
Utrecht University, PO Box 80021, 3508 TA Utrecht, The Netherlands
e-mail: joekar@geo.uu.nl, web page: http://www.geo.uu.nl/hydrogeology

†Department of Earth Sciences
Utrecht University, PO Box 80021, 3508 TA Utrecht, The Netherlands
e-mail: hassanizadeh@geo.uu.nl, web page: http://www.geo.uu.nl/hydrogeology

Key words: pore-network modeling, porous media, interfacial area

Summary. In traditional two-phase flow equations capillary pressure is simply a function of saturation. There is a hysteresis in capillary pressure-saturation curves resulted under drainage and imbibition. However, extended capillary pressure-saturation relationships suggest that there is a unique relationship among capillary pressure, saturation, and macroscopic interfacial area under drainage and imbibition. Our objective in this study is to to analyze relationship among capillary pressure, saturation, and specific interfacial area under primary drainage and main imbibition under different dynamic conditions for different viscosity ratios.

We have developed a dynamic pore-network model for two-phase drainage and imbibition experiments. To include capillary diffusion and corner flow involved in drainage and imbibition processes, angular cross sections have been assumed for the network elements, namely pore bodies and pore throats in shape of octahedron and parallelepiped, respectively. Furthermore compared with previous dynamic pore-network models, we have improvements pressure field solver as well as the algorithm for saturation update. This allows us to simulate flow dynamics under different flow regimes and viscosity ratios.

Thermodynamic-based theory of multiphase flow in porous media

Conventional equations for multiphase flow in porous media are based a central equation - capillary pressure-saturation relationship. This equation which is written based on the thermodynamically-equilibrium assumption, is commonly written as:

$$P^n - P^w = P^c(S^w) \tag{1}$$

in which, P^c is the capillary pressure, S^w is the saturation of the wetting phase, and P^n and P^w are the nonwetting and wetting phases pressures, respectively.

In fact, there are two major assumptions in this equation: a) fluid distribution and subsequently capillary pressure is a function of wetting phase saturation only, and b) fluids pressure difference is equal to capillary pressure (at all times and under all conditions). Traditional equations of multiphase flow in porous media have been challenged, primarily based on theoretical works using a thermodynamic approach by *Hassanizadeh and Gray* (1990, 1993a). They developed a theory of two-phase flow in which interfacial areas were introduced as separate thermodynamic entities, possessing mass, momentum, and energy.

Regarding the first assumption in Equation 1, it is known that there is hysteresis in P^c-S^w curves obtained for drainage and imbibition processes. *Hassanizadeh and Gray* (1993b) have suggested that the non-uniqueness in the P^c-S^w relationship is indeed due to the absence of specific interfacial area and they proposed the following equation for capillary pressure:

$$P^c(S^w) = P^c(S^w, a^{nw}) \tag{2}$$

A number of computational and experimental works have shown that under a wide range of drainage and imbibition histories, P^c-S^w-a^{nw} surfaces more or less coincide. This means that inclusion of a^{nw} leads to the removal or significant reduction of hysteresis in P^c-S^w relationship (e.g. *Chen et al.*, 2007, *Cheng et al.*, 2004, *Held and Celia*, 2001, *Joekar-Niasar et al.*, 2008, 2009, 2010a, *Porter et al.*, 2009, *Reeves and Celia*, 1996). But, all these studies are based on equilibrium configurations of the fluids and none of them has studied coincidence of P^c-S^w-a^{nw} surfaces under non-equilibrium conditions for drainage and imbibition processes.

Analysis tool

We employ pore-network modelling as an upscaling technique from pore scale to macroscale.

Dynamic pore-network model can simulate transient behaviour of flow with time for various capillary numbers and viscosity ratios. Capillary number (C_a) is traditionally defined as the ratio of viscous forces of the invading phase to capillary forces ($\frac{\mu_{inv} q_{inv}}{\sigma^{nw}}$). The first dynamic pore-network model reported in the literature was developed by *Koplik and Lasseter* (1985) to simulate imbibition process in a two-dimensional pore network. Later, several dynamic pore-network models were developed for various applications (see e.g. *Aker et al.*, 1998a,b, *Al-Gharbi and Blunt*, 2005, *Constantinides and Payatakes*, 1996, *Dahle and Celia*, 1999, *Dias and Payatakes*, 1986a,b, *Nordhaug et al.*, 2003, *Singh and Mohanty*, 2003, *Van der Marck et al.*, 1997).

Strong nonlinearity at the pore-scale causes severe numerical stability problems in dynamic pore-network models such that simulation for unfavorable viscosity ratios or for capillary-dominated flow is troublesome. In order to avoid these problems and

also to be able to simulate imbibition as well as drainage under a wide range of viscosity ratios and different flow regimes, a new computational algorithm and a robust pore-network model has been developed in *Joekar-Niasar et al.* (2010b), which employs a semi-implicit approach is used for the saturation update in order to obtain numerical stability in simulations even for capillary-dominated flow. Thus, the resulting set of equations for fluid pressures contain both advection-type terms (corresponding to viscous forces) and diffusion-type terms (corresponding to capillary forces).

Furthermore, to mimic the geometry of pore space in granular media, pore bodies and pore throats are represented as truncated octahedron and parallelepiped, respectively. Local capillary pressure is defined based on local interface curvature, which has been related to local pore body saturation. Computational and geometrial details of this DYnamic POre-network SImulator for Two-phase flow (DYPOSIT) are given in *Joekar-Niasar and Hassanizadeh* (2010), *Joekar-Niasar et al.* (2010b).

Objectives

In this paper, we investigate the following main questions:

- Evolution of average capillary pressure associated with fluid-fluid interfaces with saturation under favorable ($M \geq 1$) and unfavorable ($M < 1$) conditions for primary drainage and main imbibition processes.
- Analysis of the relationship among capillary pressure, saturation and specific interfacial area under drainage and imbibition process for favorable and unfavorable viscosity ratios.

1 MODEL DESCRIPTION

1.1 Model features

1.1.1 Structure and geometry

The pore network is a regular three-dimensional lattice with fixed coordination number of six. Pore bodies and pore throats are presented by "truncated octahedron" and "parallelepiped", respectively. This allows simultaneous existence of both phases in a single pore element. The octahedron pore bodies can be unequally truncated since they are connected to pore throats of different sizes, as shown in Figure 1(a). Truncated sections of the octahedron have the shape of square pyramids with base width of $2r_{ij}$ (which is equal to the size of pore throat ij) as shown in Figure 1(a). Cross sections through the vertices of pore bodies and the pore throat connecting them is shown in Figure 1(c). The radius of the inscribed sphere in pore body, R_i, and the radius of the inscribed circle in the cross section of pore body i, R'_i, are shown in Figure 1(b). It should be noted that $R_i = \frac{\sqrt{6}}{3} R'_i$. The size distribution of pore bodies is specified by a truncated log-normal distribution, with no spatial correlation.

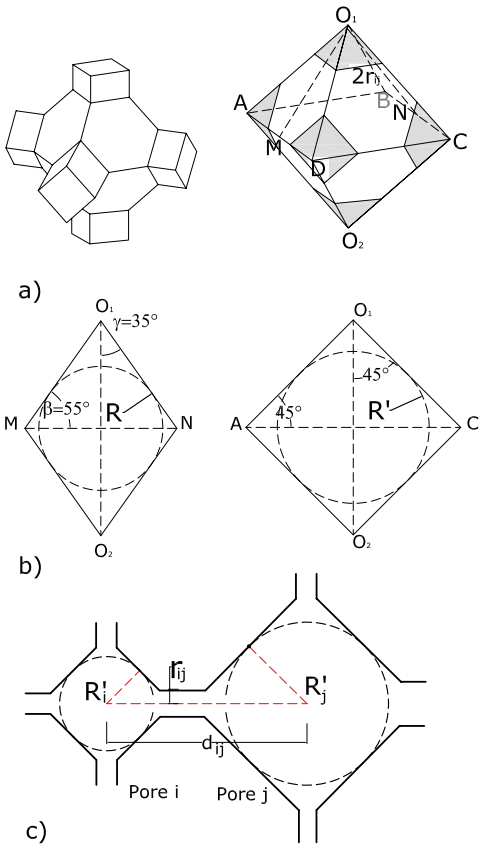

Figure 1: a) Schematic presentation of a pore body and its connected pore throats. Truncated parts of the pore body have the width of $2r_{ij}$, which is the inscribed radius of pore throat ij. b) Cross sections of the pore body along the vertices and through the edges. Radius of inscribed sphere is denoted by R and radius of inscribed circle in the cross section along vertices is denoted by R' c) Cross section of two pore bodies and connected pore throats. Geometrical configuration for determining the pore throat radius (r_{ij}) based on pore bodies radii, $R'_i = \frac{\sqrt{6}}{2} R_i$ and $R'_j = \frac{\sqrt{6}}{2} R_j$.

Pore throat radius is determined based on the pore bodies radii. Consider two pore bodies *i* and *j*, with a centre-to-centre distance d_{ij} (see Figure 1(a)), and cross section inscribed radii R'_i and R'_j, respectively. We define the dimensionless $\widetilde{R_i}$ and $\widetilde{R_j}$ as follows:

$$\widetilde{R_i} = R'_i/d_{ij}, \quad \widetilde{R_j} = R'_j/d_{ij} \tag{3}$$

We can calculate dimensionless inscribed radius of the pore throat ij, $\widetilde{r_{ij}}$, as follows:

$$\widetilde{r_{ij}} = \varrho_i \varrho_j (\varrho_i^{1/n} + \varrho_j^{1/n})^{-n}, n > 0 \tag{4}$$

$$\varrho_i = \frac{\widetilde{R}_i \sin(\pi/4)}{(1 - \widetilde{R}_i \cos(\pi/4))^n} \tag{5}$$

$$\varrho_j = \frac{\widetilde{R}_j \sin(\pi/4)}{(1 - \widetilde{R}_j \cos(\pi/4))^n} \tag{6}$$

where n is a positive number, which can control ratio between the radii of pore bodies and pore throat introduced as "aspect ratio". Larger *n* results in smaller pore throats (larger aspect ratios).

1.1.2 System parameters and specifications

Table 1 shows fluid and network properties used in the simulations. Viscosity of the nonwetting phase is kept constant equal to 0.001 and viscosity ratio is defined as the $M = \frac{\mu^n}{\mu^w}$.

Parameter	Symbol	Value	Unit
Contact angle	θ	0.0	degree
Interfacial tension	σ^{nw}	0.0725	kgs^{-2}
Wetting fluid viscosity	μ^w	0.0001,0.001, 0.01	$kgm^{-1}s^{-1}$
Non-wetting fluid viscosity	μ^n	0.001	$kgm^{-1}s^{-1}$
Total no. of pore bodies in flow direction	n_z	45	-
Total no. of pore bodies in lateral directions	n_x, n_y	35	-
Domain Size	-	1.9×1.9×2.37	mm^3
Permeability	K	1.43×10^{-12}	m^2

Table 1: Fluid and network properties used in the simulations.

Statistical properties of pore body inscribed sphere radii, pore throat inscribed circle radii, and aspect ratio distributions are shown in Table 2. Aspect ratio is defined as pore body inscribed sphere radius divided by pore throat radius. Corresponding to Table 2,

Specifications	R_i (mm)	r_{ij} (mm)	R_{asp}
min	0.0077	0.0048	1.55
max	0.0200	0.0162	4.00
mean	0.0125	0.0084	2.25
st. deviation	0.0028	0.0017	0.38

Table 2: Statistical properties of the radii of inscribed spheres in pore bodies (R_i), in pore throats r_{ij}, and aspect ratio distribution R_{asp}.

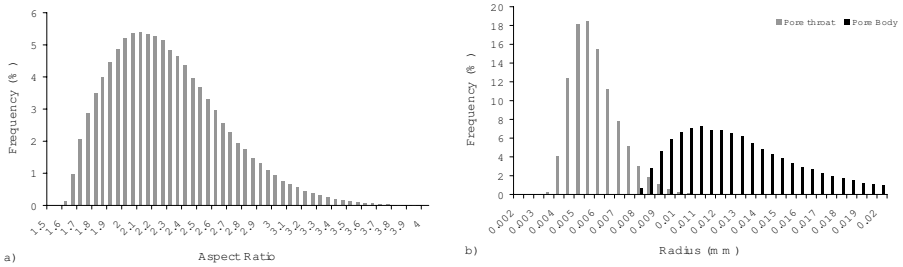

Figure 2: Network geometry properties a) Aspect ratio distribution b) Pore body and pore throat distributions.

Figures 2(a) and (b) show the aspect ratio distribution as well as pore body-pore throat size distributions, respectively .

Aspect ratio is controlled by the parameter n given in Equation 6, which is equal to $n = 1.0$ in this work.

1.2 Governing Equations

1.2.1 General equations for two-phase flow

The local capillary pressure for pore body i is defined as:

$$p_i^c = p_i^n - p_i^w = f(s_i^w) \tag{7}$$

A flux Q_{ij}^α is assigned to a pore throat ij for each phase separately. A separate volume balance for each phase in a pore body is employed:

$$V_i \frac{\Delta s_i^\alpha}{\Delta t} = -\sum_{j \in \mathrm{N}_i} Q_{ij}^\alpha, \quad \alpha = w, n \tag{8}$$

where, N_i is the set of all pore throats connected to pore body i, V_i is the volume of pore body i, s_i^α is the saturation of phase α in pore body i. The volumetric flux of phase α in pore throat ij is given by an equation similar to *Washburn* formula:

$$Q_{ij}^\alpha = -K_{ij}^\alpha \Delta p_{ij}^\alpha, \quad \alpha = w, n \tag{9}$$

where K_{ij}^{α} is a function of geometry and fluid occupancy of pore throats. Note that assigning different pressures and conductivities to each phase (as opposed to one single pressure per body and one effective conductivity per pore throat; (see e.g. *Al-Gharbi and Blunt*, 2005, *Mogensen and Stenby*, 1998) has major advantages. For example, it allows us to include mechanisms related to the local capillary pressure (such as snap-off, counter-current flow) in simulations. Equations (7), (8), and (9) form a determinate set to be solved for s_i^w, p_i^w, and p_i^n.

1.2.2 Pressure field solver

To reduce the computational demand, the general equations are reformulated in terms of a total pressure $\bar{p}_i$, defined as the saturation-weighted average of fluid pressures in a pore body:

$$\bar{p}_i = s_i^w p_i^w + s_i^n p_i^n \tag{10}$$

Combining Equations 7 and 10 and using $s_i^n + s_i^w = 1$, we get the following equations for pressures of wetting and nonwetting phases:

$$p_i^w = \bar{p}_i - s_i^n p_i^c \tag{11}$$

$$p_i^n = \bar{p}_i + s_i^w p_i^c \tag{12}$$

Substitution of Equations 11 and 12 in Equation 9 results in an equation for $\bar{p}_i$:

$$\begin{aligned} &\sum_{j\in \mathrm{N}_i} (K_{ij}^w + K_{ij}^n)(\bar{p}_i - \bar{p}_j) = \\ &-\sum_{j\in \mathrm{N}_i} [(K_{ij}^n s_i^w - K_{ij}^w(1-s_i^w))p_i^c + (K_{ij}^w(1-s_j^w) - K_{ij}^n s_j^w)p_j^c] \end{aligned} \tag{13}$$

In this equation, the right-hand side as well as the coefficients of the left-hand side depend on local saturation only. This linear system of equations was solved for $\bar{p}_i$ by diagonally-scaled biconjugate gradient method using SLATEC mathematical library (*Fong et al.*, 1993).

1.2.3 Saturation update

After calculating $\bar{p}_i$, pressures of phases can be back-calculated from Equation 11 and Equation 12, based on saturation values. Then, commonly Equation 9 can be used to calculate Q_{ij}^{α}, and using Equation 8 new saturation values can be calculated explicitly. This procedure, however, will result in numerical problems for a capillary-dominated flow regime, as mentioned in *Koplik and Lasseter* (1985). He found that the explicit saturation update was not numerically stable for very small capillary numbers and he could not successfully simulate the capillary-dominated flow. Therefore, we

have developed a semi-implicit approach, analogous to fractional flow formulation, to control the nonlinearities under such flow conditions. Details of the semi-implicit saturation update are given in *Joekar-Niasar et al.* (2010b). The resulting discretized equation reads:

$$\left(\frac{V_i}{\Delta t}-\sum_{j\in \mathrm{N}_i}\frac{K_{ij}^n K_{ij}^w}{K_{ij}^{tot}}\frac{\partial p_{ij}^c}{\partial s_{ij}^w}\right)(s_i^w)^{k+1}+\left(\sum_{j\in \mathrm{N}_i}\frac{K_{ij}^n K_{ij}^w}{K_{ij}^{tot}}\frac{\partial p_{ij}^c}{\partial s_{ij}^w}\right)(s_j^w)^{k+1}= \frac{V_i}{\Delta t}(s_i^w)^k+\sum_{j\in \mathrm{N}_i}\frac{K_{ij}^n}{K_{ij}^{tot}}Q_{ij}^{tot} \tag{14}$$

where, superscript k denotes time step level, and $\frac{\partial p_{ij}^c}{\partial s_{ij}^w}$ is calculated from the upstream pore body. One should note that since Q_{ij}^{tot} and K_{ij}^{α} are calculated from time step k, this scheme is not fully implicit. Here also the diagonally-scaled biconjugate gradient method from SLATEC mathematical library (*Fong et al.*, 1993) was used to solve Equation 15.

1.2.4 Time step

The time step is determined based on time of filling of pore bodies by the nonwetting phase or wetting phase, denoted by Δt_i. The wetting phase saturation of a pore body varies between 1 and $s_{i,min}^w$ as we assume that a pore body may be drained down to a minimum saturation. On the other hand, if local imbibition occurs, the wetting phase saturation in a pore body can go back to 1. So, we calculate Δt_i for all pore bodies, depending on the local process, from the following formulas:

$$\Delta t_i=\begin{cases}\frac{V_i}{q_i^n}(s_i^w-s_{i,min}^w) & \text{for local drainage, } q_i^n>0\\ \frac{V_i}{q_i^n}(1-s_i^w) & \text{for local imbibition, , } q_i^n<0\end{cases} \tag{15}$$

where, the accumulation rate of the nonwetting phase is defined as $q_i^n=\sum_{j\in \mathrm{N}_i}Q_{ij}^n$. Then, the global time step is chosen to be the minimum Δt_i.

$$\Delta t_{global}=min\{\Delta t_i\} \tag{16}$$

It should be noted that we imposed a truncation criterion of 10^{-6} for $s_i^w-s_{i,min}^w$ and $1-s_i^w$ in order to reduce number of solving the equations. Also note that in Equation15, there is a correspondence between saturation change (numerator) and the accumulation rate of nonwetting phase (denominator). That is, when local saturation is close to the limits, the accumulation rate of nonwetting phase is also very small. This means that Δt_i always remains finite and nonzero.

1.3 Local rules

1.3.1 Capillary pressure curves for pore bodies and pore throats

Local capillary pressure within a pore is a function of the curvature of fluid-fluid interface through *Young-Laplace* equation, regardless of whether drainage or imbibition occurs. For a given fluid-fluid interface position with in a pore body, we can determine corresponding capillary pressure and saturation. Therefore, for a given pore body, a unique relationship between capillary pressure and local saturation can be obtained. Local p_i^c-s_i^w curves for drainage and imbibition are discussed in the following sections.

Drainage During drainage, invasion of a pore throat by the nonwetting fluid is controlled by the entry capillary pressure. Thus, an interface is located within a pore body. If a pore body is filled with both fluids, the wetting phase is residing along edges of the pore bodies. The saturation of the pore body (i.e. volume of the wetting fluid divided by the volume of the pore body) depends on the prevailing capillary pressure. For a given capillary pressure, curvature of the interface in the edges of the pore body can be calculated and, consequently, the corresponding saturation can be estimated. Details of derivation of the (local) p_i^c-s_i^w relationship for an octahedron pore body have been presented in *Joekar-Niasar and Hassanizadeh* (2010).

The resulting p_i^c-s_i^w relationship in terms of the radius R_i of the inscribed sphere of the pore body i and the other geometrical parameters is:

$$p_i^c = 2\sigma^{nw}\kappa_i, \quad \kappa_i = \begin{cases} (\frac{1}{r_{ij}} - \frac{1}{R_i})(\frac{s_i^w - s_i^{dr}}{1-s_i^{dr}})^{3.5} + \frac{1}{R_i} & s_i^w \geq s_i^{dr} \\ \frac{1}{R_i}\left(\frac{s_i^w}{s_i^{dr}}\right)^a, a = \frac{1}{2.98 s_i^{dr} - 3.85} & s_i^{min} < s_i^w < s_i^{dr} \end{cases} \tag{17}$$

in which, s_i^{dr} is the wetting fluid saturation corresponding to the inscribed sphere given by the following equation:

$$s_i^{dr} = 1 - \frac{\pi R_i^3}{3\sqrt{3}R_i^3 - \sqrt{2}\sum_{j\in \mathrm{N}_i} r_{ij}^3} \tag{18}$$

, s_i^{min} is the minimum possible saturation in a simulation given by Equation 19, and r_{ij} is the pore throat inscribed radius.

Obviously it is impossible to completely displace the wetting phase from the corners of a pore body. We assume that each pore body has a minimum saturation $s_{i,min}^w$, that depends on the imposed global pressure difference (P_{global}^c defined in §2.2) as well as the blockage of the invading fluid. The capillary blockage of invading fluid ($P_{e_{block}}^c$) is also a global variable, defined to be the minimum entry capillary pressure of all pore throats that are in the vicinity of the nonwetting phase but not invaded by it yet. Thus, using the p_i^c-s_i^w relationship given by Equation17, the local minimum wetting phase

saturation in a pore body may be determined as follows:

$$s^w_{i,min} = s^{dr}_i \left(\frac{R_i}{2\sigma^{nw}} \min\{P^c_{global}, P^c_{e_{block}}\} \right)^{2.98 s^{dr}_i - 3.85} \tag{19}$$

A capillary pressure should be also assigned to a pore throat once it is invaded and both phases are present. We assume that capillary pressure in a pore throat is equal to the capillary pressure of the upstream pore body.

Imbibition We define local capillary pressure-saturation relationship as a function of saturation as well as pore throats filling to consider effect of cooperative fillying. Details of derivation of local p^c_i-s^w_i relationship during imbibition are given in *Joekar-Niasar and Hassanizadeh* (2010). They have suggested the following relationships for a truncated octahedron pore body:

$$p^c_i = 2\sigma^{nw}\kappa_i, \quad \kappa_i = \begin{cases} \left(\frac{1}{r_{ij}} - \frac{1}{R_i}\left(\frac{s^{imb}_i}{s^{dr}_i}\right)^a\right)\left(\frac{s^w_i - s^{imb}_i}{1 - s^{imb}_i}\right)^{3.5} + \frac{1}{R_i}\left(\frac{s^{imb}_i}{s^{dr}_i}\right)^a & s^w_i \geq s^{imb}_i \\ \frac{1}{R_i}\left(\frac{s^w_i}{s^{dr}_i}\right)^a, a = \frac{1}{2.98 s^{dr}_i - 3.85} & s^{min}_i < s^w_i < s^{imb}_i \end{cases} \tag{20}$$

where s^{imb}_i is the pore body saturation at which one pore throat is still filled with the nonwetting phase.

1.3.2 Interfacial area versus saturation in a pore body

Interfacial area under drainage and imbibition has been determined differently. Under drainage three zones have been defined: a) local wetting saturation is larger than inscribed sphere ($s^{dr}_i < s^w_i$), b) local saturation is smaller than inscribed sphere volume but at least one of the pore throats has not been invaded. c) residual saturation, where all pore throats have been invaded ($s^w_i < s^w_i(\kappa^{dr}_i)$).

$$A^{nw}_i(mm) = \begin{cases} \frac{1}{2\kappa_i}(0.6155 - \theta)\left(12\sqrt{6}R_i - 8\sum_{j\in \mathrm{N}_i} r_{ij}\right) & s^w_i < s^w_i(\kappa^{dr}_i) \\ A^{nw}_{dr} + (4\pi R^2_i - A^{nw}_{dr})\left(\frac{\kappa_i - \kappa^{dr}_i}{R_i - \kappa^{dr}_i}\right) & s^w_i(\kappa^{dr}_i) \leq s^w_i < s^{dr}_i \\ \frac{4\pi}{\kappa^2_i} & s^{dr}_i < s^w_i \end{cases} \tag{21}$$

Similar to the equation above, an equation for imbibition can be used. The only difference is the criterion for s^{imb}_i as shown below.

$$A^{nw}_i(mm) = \begin{cases} \frac{1}{2\kappa_i}(0.6155 - \theta)\left(12\sqrt{6}R_i - 8\sum_{j\in \mathrm{N}_i} r_{ij}\right) & s^w_i < s^w_i(\kappa^{dr}_i) \\ A^{nw}_{dr} + (4\pi R^2_i - A^{nw}_{dr})\left(\frac{\kappa_i - \kappa^{dr}_i}{R_i - \kappa^{dr}_i}\right) & s^w_i(\kappa^{dr}_i) \leq s^w_i < s^{imb}_i \\ \frac{4\pi}{\kappa^2_i} & s^{imb}_i < s^w_i \end{cases} \tag{22}$$

1.3.3 Entry capillary pressure for a pore throat

We assume that a pore throat will be invaded by the nonwetting phase when the capillary pressure in a neighboring pore body becomes larger than the entry capillary pressure of the pore throat. For a pore throat with square cross section, the entry capillary pressure can be calculated as follows (due to *Ma et al.*, 1996, *Mayer and Stowe*, 1965, *Princen*, 1969a,b, 1970):

$$p^c_{e,ij} = \frac{\sigma^{nw}}{r_{ij}} \left(\frac{\theta + \cos^2\theta - \pi/4 - \sin\theta\cos\theta}{\cos\theta - \sqrt{\pi/4 - \theta + \sin\theta\cos\theta}} \right) \tag{23}$$

where r_{ij} is the radius of inscribed circle of the pore throat cross section, and θ is the contact angle.

1.3.4 Conductivities of pore throats

Conductivities of pore throats are determined based on their size and fluid occupancy. One of the following two cases may occur.

a) A pore throat is occupied by the wetting phase only. For this case, the following equation was obtained by *Azzam and Dullien* (1977):

$$\begin{aligned} K^w_{ij} &= \frac{\pi}{8\mu^w l_{ij}} (r^{eff}_{ij})^4 \\ K^n_{ij} &= 0 \end{aligned} \tag{24}$$

where μ^w is the viscosity of the wetting phase, l_{ij} is the length of pore throat, and

$$r^{eff}_{ij} = \sqrt{\frac{4}{\pi}} r_{ij} \tag{25}$$

b) A pore throat is occupied by both phases. Then, following *Ransohoff and Radke* (1988) we can write:

$$K^w_{ij} = \frac{4-\pi}{\beta\mu^w l_{ij}} (r^c_{ij})^4 \tag{26}$$

$$K^n_{ij} = \frac{\pi}{8\mu^n l_{ij}} (r^{eff}_{ij})^4 \tag{27}$$

where

$$r^c_{ij} = \frac{\sigma^{nw}}{p^c_{ij}} \tag{28}$$

$$r^{eff}_{ij} = \frac{1}{2} \left(\sqrt{\frac{r^2_{ij} - (4-\pi) r^{c^2}_{ij}}{\pi}} + r_{ij} \right) \tag{29}$$

In (26), β is a resistance factor that depends on geometry, surface roughness, crevice roundness and other specifications of the cross section. Detailed explanation about β can be found in *Zhou et al.* (1997). As mentioned earlier, the pore throat capillary pressure p^c_{ij} is set equal to the capillary pressure of the upstream pore body.

1.3.5 Snap-off

If the local capillary pressure in a pore throat becomes smaller than a critical value (defined below), the corner interfaces become unstable and snap-off will occur. The criterion for snap-off in a square cross section pore throat has been defined as follows (*Vidales et al.*, 1998):

$$p^c_{ij} \leq \frac{\sigma^{nw}}{r_{ij}}(\cos\theta - \sin\theta) \tag{30}$$

We assume that as soon as snap-off occurs, the nonwetting phase retreats instantaneously into the two neighboring pore bodies, and the pore throat is filled up with the wetting phase.

2 SIMULATIONS AND ANALYSIS

2.1 Network size

To analyze Darcy-scale equations using pore-network models, size of the pore-network should be at least one REV. REV size was determined by performing quasi-static drainage simulations in networks with different sizes but the same statistical parameters. Our simulations show that the REV size for these statistical parameters is a cube with length of 35 pore bodies. However, we have added five buffer layers at each boundary to reduce the boundary effect. Thus the network has a length of 45 pore bodies along the main flow direction and these buffer layers are not included in the averaging window.

2.2 Boundary conditions

For our simulations, we assume that the network is connected to a nonwetting phase reservoir on one side and a wetting phase reservoir on the other side. Phase pressures are specified at these boundaries. Side boundary conditions are assumed to be periodic.

For drainage and imbibiton simulations the following procedure is followed:

a) Drainage: Pressure at the nonwetting phase reservoir is fixed to P^n_{top} and pressure at the wetting phase reservoir is fixed to zero. The difference between the two boundary pressures during drainage is referred to as "global pressure difference" P^c_{global}. After the invasion of a pore throat at the wetting-phase boundary by the nonwetting phase, it is assumed that the gradient of capillary pressure within the invaded pore throat is equal to zero. In other words, we assign nonwetting phase pressure at the

downstream of pore throat equal to the nonwetting phase pressure that the upstream of pore throat.

b) Imbibition: Similar to the drainage process, pressure at the nonwetting phase reservoir is fixed to P^n_{top} and pressure at the wetting phase reservoir is fixed to zero. However, P^n_{top} should be so small that imbibition process can occur continuously. During imbibition similar to the drainage, it is assumed that $\frac{\partial p^c_{ij}}{\partial x} = 0$ as long as a pore throat at the nonwetting phase boundary is filled with both fluids.

2.3 Drainage simulations

For primary drainage, the network is initially fully saturated with the wetting phase. Simulation of drainage starts with raising the pressure of the nonwetting phase reservoir, and establishing a global pressure difference, P^c_{global}, across the network. When the pressure difference is larger than the entry pressure of the largest pore throat connected to the nonwetting phase reservoir, drainage starts. In quasi-static simulations, the nonwetting phase reservoir pressure is increased in incremental steps so that the network is invaded in steps. At the end of each step, when there is no flow (static conditions), the overall saturation of the network is determined. Then, global pressure difference is increased again. In dynamic simulations, the imposed P^c_{global} is so large that the whole network could be flooded. The simulations are continued till change of average saturation in a selected averaging window is not significant.

For main drainage simulations, the initial saturation occupancy is based on the last snapshot of the quasi-static main imbibition experiment. The simulation procedure is otherwise similar to the primary drainage simulation.

2.4 Imbibition simulations

Consider a pore network filled by the nonwetting phase at the end of a drainage experiment. The wetting phase is still present along edges of pore bodies and pore throats. Starting from an equilibrium condition, all pore bodies have the same capillary pressure. The global capillary pressure is decreased by reducing the nonwetting-phase reservoir pressure or increasing the wetting-phase reservoir pressure. A decrease in the global capillary pressure causes the interfaces to relax gradually and main imbibition experiment will start. The imbibition simulation will stop when all pore throats at the outflow boundary (nonwetting phase reservoir) are fully filled with the wetting phase.

For the quasi-static imbibition simulations, an approach similar to the drainage has been employed.

2.5 Averaging procedure

Our simulations result in local-scale variables such as pressure, saturation, and fluxes. These have to be averaged over the averaging window to obtain macroscopic variables. Average saturation is simply defined the ratio of the wetting phase to the

total pore volume of the network:

$$S^w = \frac{V^w}{V^w + V^n} = \frac{\sum_{i=1}^{n_{pb}} s_i^w V_i}{\sum_{i=1}^{n_{pb}} V_i} \qquad (31)$$
$$S^n = 1 - S^w$$

in which n_{pb} is the total number of pore bodies. Specific interfacial area is calculated using the following equation:

$$a^{nw} = \frac{\sum_{i=1}^{n_{pb}} A_i^{nw}}{V_{network}} \qquad (32)$$

We calculate average capillary pressure as follows:

$$P^c = \frac{\sum_{i=1}^{n_{pb}} p_i^c A_i^{nw}}{\sum_{i=1}^{n_{pb}} A_i^{nw}} \qquad (33)$$

2.6 Effect of viscosity ratio on fluid distribution

Fluid entrapment at pore scale and subsequently fluid distribution at macro-scale is controlled by pore scale invasion mechanisms, such as piston-like movement, snap-off, etc. Depending on the process (drainage or imbibition) importance of these mechanisms can vary. For instance, snap-off during drainage is not as important as during imbibition, since during imbibition nonwetting phase is the receding phase. As a result, at the end of imbibition process, a significant amount of the nonwetting phase remains behind as residual saturation. Due to the importance of imbibition in reservoir engineering, dependence of residual saturation on capillary number, viscosity ratio, contact angle and pores aspect ratio has been studied significantly (see e.g. *Dias and Payatakes*, 1986a,b, *Hughes and Blunt*, 2000, *Mogensen and Stenby*, 1998, *Vizika et al.*, 1994).

In this section, the effects of capillary number, global pressure difference, and viscosity ratio on snap-off and residual saturation and saturation profile are studied. Because in simulations with constant boundary pressure, capillary changes continuously, first we performed some additional imbibition simulations with constant wetting phase flux specified as the wetting phase boundary condition and constant pressure at the nonwetting phase boundary. By performing imbibition simulations at various fluxes, the nonwetting phase residual saturation was determined as a function of capillary number (plotted in Figure 3), for the case of equal fluid viscosities ($M = 1.0$). This figure shows that with increase of capillary number, the residual nonwetting phase saturation decreases. The largest decrease occurs for capillary numbers between 10^{-6} and 10^{-4}. At higher capillary numbers, the snap-off mechanism is suppressed.

In our main simulations, with constant boundary pressure, capillary number varied significantly as imbibition occurred. This is made apparent in Figure 4, where capillary number is plotted for various viscosity ratios and global pressure difference values as

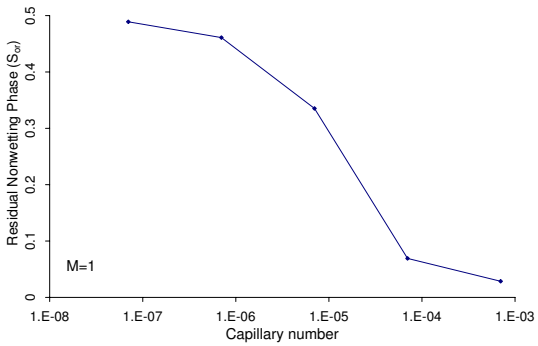

Figure 3: Effect of capillary number on residual nonwetting saturation for $M = 1.0$.

a function of wetting phase saturation during imbibition. It is evident that the largest variation occurs in the case of $M = 10$. This case is also the most sensitive to the global pressure difference. A larger global pressure difference results in higher capillary number and thus a lower residual nonwetting phase saturation. This is because with the increase of capillary number, probability of snap-off decreases and consequently flooding efficiency increases.

Similar effects can be observed when examining the average saturation profile along the network, shown in Figure 5. Here, the saturation is averaged over a cross section of the network located at position x and then plotted against x/l at different times, and for two different viscosity ratios. An interesting result here is the non-monotonic behavior of saturation for $M = 10$. This is because snap-off is suppressed with invasion of the wetting phase as the capillary number increases. Moreover, the saturation front for the case of $M = 10$ is steeper than for $M = 1.0$. This is because for $M = 10$, the resident nonwetting-phase is more viscous than for $M = 1.0$ and local imbibition is resisted. The fact that viscosity ratio greatly affects fluid occupancy in the network is illustrated in Figure 5(c) where the histogram of the local pore body saturation at the end of imbibition process, for $\Delta P = -10kPa$, is shown. It is clear that with decrease of viscosity ratio (viscous wetting fluid), less snap-off occurs and more flooding efficiency is resulted.

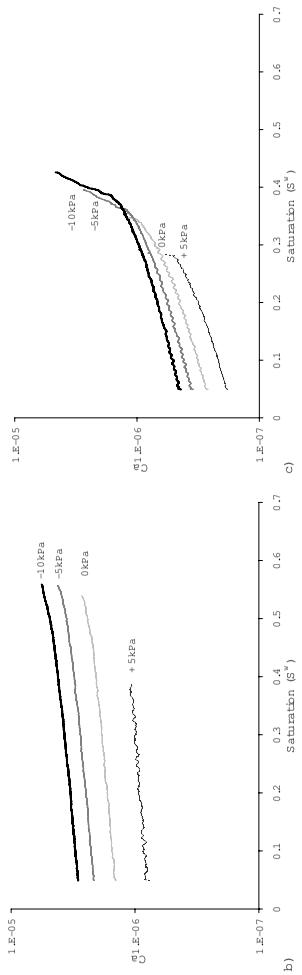

Figure 4: Variation of capillary number during imbibition under constant pressure boundary conditions for a) $M = 0.1$,b) $M = 1.0$,a) $M = 10$ and $M = \mu^n/\mu^w$. With decrease of nonwetting phase saturation for $M = 1.0$ and $M = 10$, flow rate of wetting phase increases.

To show the effect of viscosity ratio on saturation profile during drainage, saturation profiles for $M = 1.0$ and 0.1 for $\Delta P = 45kPa$ have been shown in Figure 6. As it can be seen, for $M = 0.1$ the invading front is unstable and the slope of the front is much smaller than for $M = 1.0$. Comparison between invasion front for these two cases shows how significant is the effect of local heterogeneities in porous medium on saturation profile. Consequently, the flooding efficiency is smaller in $M = 0.1$ compared with $M = 10$. However, due to the fact that during imbibition snap-off is the major mechanism that controls the entrapment of the nonwetting phase, effect of viscosity ratio on residual saturation is more significant during imbibition than drainage.

2.7 Relationship among P^c, S^w, and a^{nw} under non-equilibrium conditions

The transient capillary pressure-saturation curves depend strongly on global capillary pressure and viscosity ratio, as shown in Figures 7(a) and 8(a). Behavior of capillary pressure versus saturation under non-equilibrium conditions is different from quasi-static curves. This difference is more pronounced under imbibition compared to drainage process. Under imbibition conditions, there is no sudden drop of capillary pressure under non-equilibrium conditions compared with the equilibrium conditions. These is due to the fact that at the beginning of imbibition process, all the interfaces are pinched into the corners (which causes a large capillary pressure). Those interfaces can be relaxed, which are close to the wetting fluid. Thus, with graduation invasion of the wetting fluid, more interfaces will be relaxed. This trend, which is gradual, depends on the viscosity ratio and global capillary pressure. Smaller global capillary pressure and smaller viscosity ratios result in steeper drop of capillary pressure versus saturation as shown in Figure 8(a). These figures show that there is no unique capillary pressure-saturation curve and obviously there should be another effective parameter that is variable. Since *Hassanizadeh and Gray* (1993a) suggested specific interfacial area as a new variable that should be included, we have plotted a^{nw}-S^w relationships for drainage and imbibition processes in Figures 7(b) and 8(b), respectively. As it is obvious, these curves similar to P^c-S^w curves depend also on global capillary pressure and viscosity ratio. One should note that specific interfacial area plotted here includes arc menisci area as well as main terminal menisci area. Depending on the angularity of the system, magnitude of specific interfacial area can change, but the qualitative behavior and its non-equilibrium dependence does not change *Joekar-Niasar et al.* (2010a). With decrease of viscosity ratio, more interfacial area is created, which is in agreement with *Joekar-Niasar et al.* (2010a). Effect of viscosity ratio on specific interfacial area is more pronounced during imbibition compared with drainage. This is due to fact that the effect of viscosity ratio on flooding efficiency is more important during imbibition compared to the drainage (snap-off effect). As it is known, under unfavorable conditions, flooding efficiency decreases (trapping increases). The increase of trapping causes increase of interfacial area.

Finally we can plot all the drainage and imbibition data points on two surfaces,

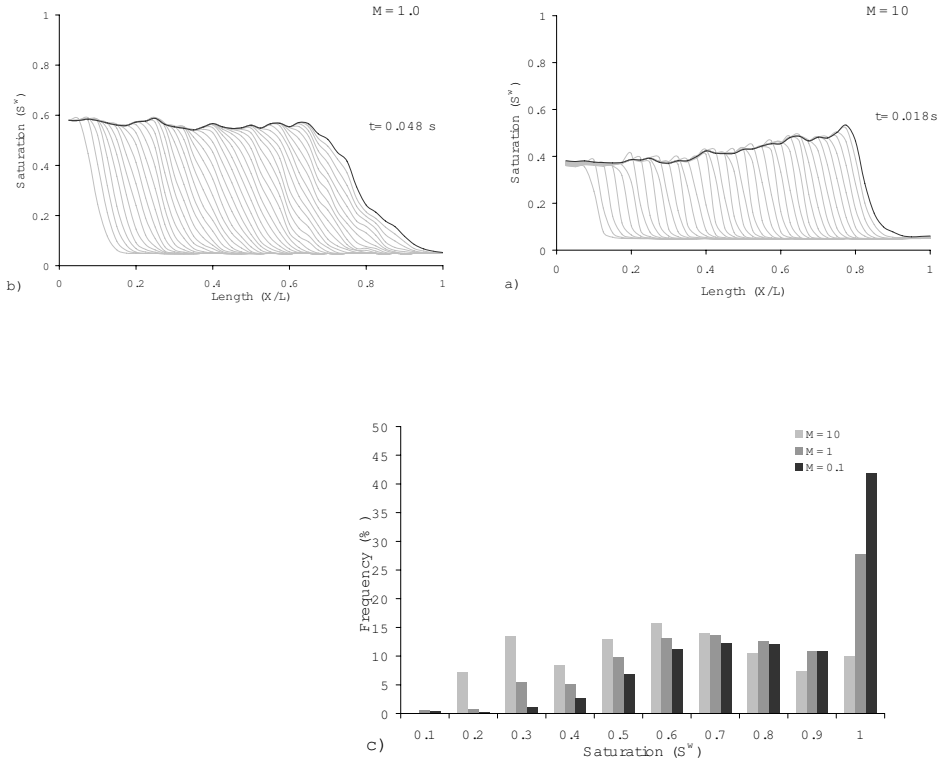

Figure 5: Wetting phase saturation profiles for $\Delta P = -10kPa$ for a) $M = 10$ and b) $M = 1$. Dark-colored curves show the wetting phase saturation distribution at the time of breakthrough of the wetting phase. Light-colored curves show the saturation profile at earlier times. c) Distribution of local saturation of pore bodies at the end of main imbibition simulations for $M = 0.1, 1, 10$ for $\Delta P = -10kPa$. For $M = 0.1$, more pore bodies are fully imbibed compared with $M = 1$ and 10.

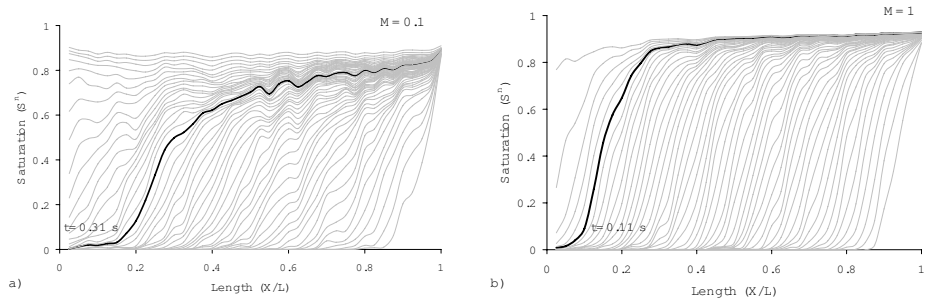

Figure 6: Effect of viscosity ratio on invasion process during drainage. Traveling wave of saturation during dranage for $\Delta P = 45kPa$ for a) $M = 0.1$ and b) $M = 1$. For $M = 0.1$ the invasion front is unstable and effect of porous medium topology to create viscous fingering is obvious.

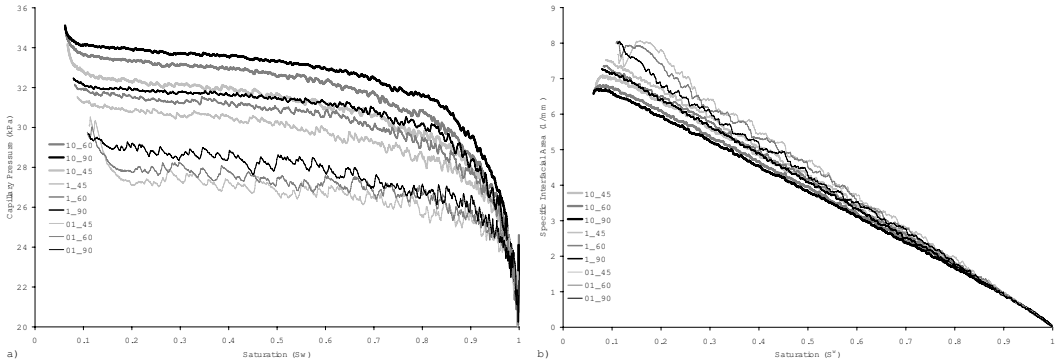

Figure 7: a) P^c-S^w, and b) a^{nw}-S^w non-equilibrium curves for drainage process for different global capillary pressures (P^c_{global} =45, 60, 90 kPa) and different viscosity ratios (M =0.1,10,10).

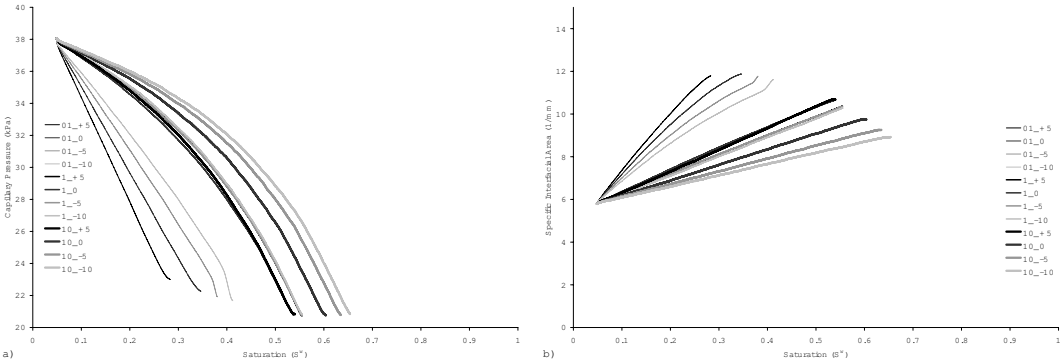

Figure 8: a) P^c-S^w, and b) a^{nw}-S^w non-equilibrium curves for imbibition process for different global capillary pressures (P^c_{global} =+5,0, -5, -10 kPa) and different viscosity ratios (M =0.1,10,10).

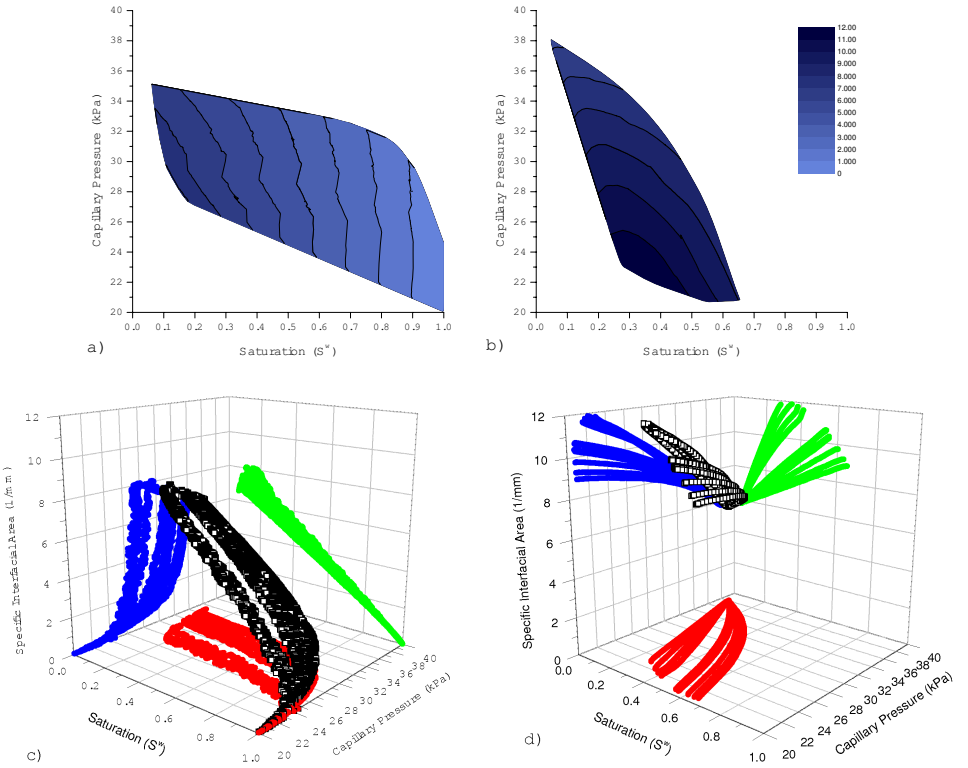

Figure 9: Contour maps for specific interfacial area versus saturation and capillary pressure for a) drainage b) imbibition. 3D presentations of all data points resulted from c) drainage and d) imbibition simulations.

separately. Contour maps and three-dimensional presentations of interfacial area for given capillary pressures and saturations are shown in Figure 9. As it can be observed, all data points resulted from drainage simulations create a well-behaved surface. This trend is less visible for imbibition curves due to limited range of data points. However, there is still a smooth surface generated by imbibition data points. The contour maps shown in Figures 9(a) and (b) show a qualitative reasonable trend in variation of specific interfacial area. As it can be seen in both curves the contour lines incline downwards toward the x-axis. Furthermore, with increase of wetting fluid saturation, magnitude of interfacial area decreases. Since the range of imbibition data points is limited it is difficult to propose the uniqueness of the drainage and imbibition P^c-S^w-a^{nw} surfaces. The overlapping parts of the contour maps show a decrease in hysteresis observed in P^c-S^w curves for drainage and imbibition.

3 CONCLUSION

We have employed a dynamic pore-network model, called DYPOSIT, to investigate qualitative behavior of macroscopic fluid-fluid interfacial area under non-equilibrium

conditions. The pore-network model consists of truncated octahedron pore bodies and parallelepiped pore throats. The angularity in cross sections allows for simultaneous flow of both nonwetting and wetting fluids. This means that capillary diffusion in the network is properly taken into account. The pressure field is computed for each phase separately to consider counter-current flow within pore throats. To improve numerical stability of the model under capillary dominated flow, a semi-implicit algorithm is employed. This allows us to simulate flow dynamics for different flow regimes and viscosity ratios for drainage as well as imbibition.

We have shown that there is no unique capillary pressure-saturation curve. This curve depends on dynamics of the system, namely global pressure difference and viscosity ratio. Under unfavorable conditions more fluid interfacial area can be created. This effect is strongly pronounced under imbibition process, where complicated pore-scale mechanisms, such as snap-off and cooperative filling occur. All data points plotted for drainage and imbibition simulations (under different dynamic conditions) create well-behaved P^c-S^w-a^{nw} surfaces. These surfaces are qualitatively in agreement with each other in terms of variation of interfacial area with capillary pressure and saturation. A very important remark is that all the cross sections of network elements are angular. This feature of the model provides the possibility of snap-off in all network elements, which leads to a very complicated invasion process especially during imbibition. Since accurate simulation of snap-off and cooperative filling during imbibition using dynamic pore-network models is not straight forward, there are some simplifications in the modeling procedure. Nevertheless, there is still a reasonable agreement between P^c-S^w-a^{nw} contour maps resulted from drainage and imbibition processes.

References

Aker, E., J. Maloy, A. Hansen, and G. G. Batrouni (1998a), A two-dimensional network simulator for two-phase flow in porous media, *Transport in Porous Media*, *32*, 163–186.

Aker, E. K., K. J. Maloy, and A. Hansen (1998b), Simulating temporal evolution of pressure in two-phase flow in porous media, *Physical Review E*, *58*, 2217–2226.

Al-Gharbi, M. S., and M. J. Blunt (2005), Dynamic network modeling of two-phase drainage in porous media, *Phys Rev E Stat Nonlin Soft Matter Phys*, *71*, 016,308 – 016,308, doi:10.1103/PhysRevE.71.016308.

Azzam, M. I. S., and F. A. L. Dullien (1977), Flow in tubes with periodic step changes in diameter: a numerical solution, *Chem. Eng. Sci.*, *32*, 1445–1455.

Chen, D. Q., L. J. Pyrak-Nolte, J. Griffin, and N. J. Giordano (2007), Measurement of interfacial area per volume for drainage and imbibition, *Water Resources Research*, *43*, W12,504, doi:10.1029/2007WR0060217.

Cheng, J. T., L. J. Pyrak-Nolte, and D. D. Nolte (2004), Linking pressure and saturation through interfacial area in porous media, *Geophysical Research Letters*, *31*, L08,502, doi:10.1029/2003GL019282.

Constantinides, G. N., and A. C. Payatakes (1996), Network simulation of steady-state two-phase flow in consolidated porous media, *AIChE Journal*, *42*, 369–382.

Dahle, H. K., and M. A. Celia (1999), A dynamic network model for two-phase immiscible flow, *Computational Geosciences*, *3*, 1–22.

Dias, M. M., and A. C. Payatakes (1986a), Network models for two-phase flow in porous media part 1. immiscible microdisplacement of non-wetting fluids, *J. Fluid Mechanics*, *164*, 305–336.

Dias, M. M., and A. C. Payatakes (1986b), Network models for two-phase flow in porous media part 2. motion of oil ganglia, *J. Fluid Mechanics*, *164*, 337–358.

Fong, K. W., T. H. Jefferson, T. Suyehiro, and L. Walton (1993), Guide to the slatec common mathematical library.

Hassanizadeh, S. M., and W. G. Gray (1990), Mechanics and thermodynamics of multiphase flow in porous media including interphase boundaries, *Advances in Water Resources*, *13*, 169–186.

Hassanizadeh, S. M., and W. G. Gray (1993a), Thermodynamic basis of capillary pressure in porous media, *Water Resources Research*, *29*, 3389–3405.

Hassanizadeh, S. M., and W. G. Gray (1993b), Toward an improved description of the physics of two-phase ow., *Advances in Water Resources*, *16*, 53–67.

Held, R. J., and M. A. Celia (2001), Modeling support of functional relationships between capillary pressure, saturation, interfacial area and common lines, *Advances in Water Resources*, *24*, 325–343.

Hughes, R. G., and M. J. Blunt (2000), Pore scale modeling of rate effect in imbibition, *Transport in Porous Media*, *40*, 295–322.

Joekar-Niasar, V., and S. M. Hassanizadeh (2010), Effect of fluids properties on non-equilibrium capillarity effects; dynamic pore-network modelling, *International Journal of Multiphase Flow*, p. submitted.

Joekar-Niasar, V., S. Hassanizadeh, and A. Leijnse (2008), Insights into the relationships among capillary pressure, saturation, interfacial area and relative permeability using pore-network modeling, *Transport in Porous Media*, *74*(2), 201–219.

Joekar-Niasar, V., S. M. Hassanizadeh, L. J. Pyrak-Nolte, and C. Berentsen (2009), Simulating drainage and imbibition experiments in a high-porosity micromodel using an unstructured pore network model, *Water Resources Research*, *45*, W02,430, doi: 10.1029/2007WR006641.

Joekar-Niasar, V., M. Prodanović, D. Wildenschild, and S. M. Hassanizadeh (2010a), Network model investigation of interfacial area, capillary pressure and saturation relationships in granular porous media, *Water Resources Research*, p. in press, doi: 10.1029/2009WR008585.

Joekar-Niasar, V., S. M. Hassanizadeh, and H. K. Dahle (2010b), Non-equilibrium effects in capillarity and interfacial area in two-phase flow: Dynamic pore-network modelling, *Journal of Fluid Mechanics*, *accepted*, XX.

Koplik, J., and T. J. Lasseter (1985), Two-phase flow in random network models of porous media, *Society of Petroleum Engineers Journal*, *25*, 89–110, doi:10.2118/11014-PA.

Ma, S., G. Mason, and N. R. Morrow (1996), Effect of contact angle on drainage and imbibition in regular polygonal tubes, *Colloids and Surfaces A.*, *117*, 273–291.

Mayer, R. P., and R. A. Stowe (1965), Mercury porosimetry-breakthrough pressure for penetration between packed spheres, *J. Colloid Sci.*, *20*, 891–911.

Mogensen, K., and E. H. Stenby (1998), A dynamic two-phase pore-scale model for imbibition, *Transport in Porous Media*, *32*, 299–327.

Nordhaug, H. F., M. Celia, and H. K. Dahle (2003), A pore network model for calculation of interfacial velocities, *Advances in Water Resources*, *26*, 1061–1074.

Porter, M. L., M. G. Schaap, and D. Wildenschild (2009), Lattice-boltzmann simulations of the capillary pressure-saturation-interfacial area relationship for porous media, *Advances in Water Resources*, *32*(11), 1632 – 1640, doi:DOI: 10.1016/j.advwatres.2009.08.009.

Princen, H. M. J. (1969a), Capillary phenomena in assemblies of parallel cylinders i.capillary rise between two cylinders, *Colloid Interface Sci.*, *30*, 69–75.

Princen, H. M. J. (1969b), Capillary phenomena in assemblies of parallel cylinders ii.capillary rise in systems with more than two cylinders, *Colloid Interface Sci.*, *30*, 359–371.

Princen, H. M. J. (1970), Capillary phenomena in assemblies of parallel cylinders iii.liquid columns between horizontal parallel cylinders, *Colloid Interface Sci.*, *34*, 171–184.

Ransohoff, T. C., and C. J. Radke (1988), Laminar flow of a wetting liquid along the corners of a predominantly gas-occupied noncircular pore, *J. Coll. Int. Sci.*, *121*, 392–401.

Reeves, P. C., and M. A. Celia (1996), A functional relationship between capillary pressure, saturation, and interfacial area as revealed by a pore-scale network model, *Water Resources Research*, *32*, 2345–2358.

Singh, M., and K. K. Mohanty (2003), Dynamic modelling of drainage through three-dimensional porous materials, *Chem Eng Sci*, *58*, 1–18.

Van der Marck, S. C., T. Matsuura, and J. Glas (1997), Viscous and capillary pressures during drainage: Network simulations and experiments, *Physical Review E*, *56*, 5675–5687.

Vidales, A. M., J. L. Riccardo, and G. Zgrabli (1998), Pore-level modelling of wetting on correlated porous media, *J. Phys. D, Appl. Phys.*, *31*, 2861–2868.

Vizika, O., D. G. Avraam, and A. C. Payatakes (1994), On the role of viscosity ratio during low-capillary-number forced imbibition in porous media, *Journal of Colloid and Interface Science*, *165*, 386–401.

Zhou, D., M. J. Blunt, and F. M. Orr (1997), Hydrocarbon drainage along corners of noncircular capillaries, *J. Coll. Int. Sci.*, *187*, 11–21.